Mathematical Biosciences 262 (2015) 206–213

Contents lists available at ScienceDirect

Mathematical Biosciences

journal homepage: www.elsevier.com/locate/mbs

A comprehensive mathematical framework for modeling intestinal smooth muscle cell contraction with applications to intestinal edema

Jennifer Young, Sevtap Ozisik*, Beatrice Riviere, Muhammad Shamim

Computational and Applied Mathematics Department, Rice University, Houston, Texas 77005, USA

ARTICLE INFO

Article history:
Received 22 May 2014
Revised 11 December 2014
Accepted 18 December 2014
Available online 30 January 2015

Keywords:
Smooth muscle
Edema
Intestine
Contraction
Simulation

ABSTRACT

The contraction of intestinal smooth muscle cells (ISMCs) involves many coordinated biochemical and mechanical processes. In this work, we present a framework for modeling ISMC contractility that begins with chemical models of calcium dynamics, continues with myosin light chain phosphorylation and force generation, and ends with a cell model of the ISMC undergoing contraction–relaxation. The motivation for developing this comprehensive framework is to study the effects of edema (excess fluid build-up in the muscle tissue) on ISMC contractility. The hypothesis is that more fluid equates to dilution of an external stimulis, eventually leading to reduced contractility. We compare our results to experimental data collected from normal versus edematous intestinal muscle tissue.

1. Introduction

The coordinated contraction of intestinal smooth muscle cells (ISMCs) is a complex process, regulated by several systems, including the enteric nerve system (ENS), the interstitial cells of Cajal (ICC), and the smooth muscle cells themselves. The entire process includes many chemical reactions and mechanical triggers working in series and in parallel to produce the contraction–relaxation cycle. Due to its complexity, it is often experimentally difficult to isolate the effect of one factor on the overall process [1,2]. Mathematical modeling offers a different perspective to the problem, allowing one to test various combinations of parameters and structural geometries to assess their effects on the process [1,2]. In this work we present a comprehensive mathematical framework of the contraction of an ISMC from calcium dynamics to the end-product mechanical contraction. The model includes several coupled sets of biochemical reactions as well as a cell model of the ISMC as it undergoes contraction–relaxation. This work incorporates both chemical and cell models together.

A motivating factor for developing such a model is to understand the effects that a medical condition known as intestinal edema may have on ISMC contractility. Intestinal edema refers to the excess accumulation of fluid in the interstitial spaces between tissue cells of the intestinal wall [3,4]. This condition can occur as a result of gastrointestinal diseases such as gastroschisis, inflammatory bowel disease, and cirrhosis [5]. This interstitial swelling of the intestinal tissue is problematic because it often leads to ileus, a decrease in intestinal transit due to a decrease in ISMC contractility [6,7]. The link between edema and ileus is unknown and is the subject of current experimental research [5–9]. One idea is that the increase in fluid volume creates larger distances over which neurotransmitters must diffuse, diluting their transmission, consequently leading to reduced contractility. We test this hypothesis with the model presented in this paper, and utilize the experimental data of Uray et al. [8] as a means of validation.

A brief summary of the processes involved in ISMC contraction will now be presented, with further details given in later sections that coincide with the various parts of the mathematical model. ISMCs are organized into two concentric layers: circular and longitudinal. A layer of connective tissue and neurons termed the myenteric plexus is situated in between the two muscle layers [10]. These neurons (part of the ENS) release neurotransmitters from axon varicosities that are transmitted via synapses to nearby muscle cells and ICCs [1]. Once a neurotransmitter binds to the postsynaptic membrane, a series of chemical reactions begins, leading to an increase in intracellular calcium ions (Ca^{2+}) [11–13]. The rise in Ca^{2+} initiates another set of reactions, leading to myosin light chain (MLC) phosphorylation [14]. Myosin is a force-generating motor protein in ISMCs. Myosin filaments form cross-bridges with actin filaments that are attached to the ISMC membrane. The myosin filaments pull on these actin filaments in a coordinated fashion, contracting the ISMC [15,16]. Once Ca^{2+} levels begin to decrease, the ISMC relaxes, and the cycle is complete.

Previous models of intestinal smooth muscle contraction have focused on a subset of the processes involved in the overall process. The excitation of the cell by these neurotransmitters that leads to

* Corresponding author. Tel.: +1 7135609766.
E-mail address: so2@rice.edu, ozisik.sevtap@gmail.com (S. Ozisik).

http://dx.doi.org/10.1016/j.mbs.2014.12.009
0025-5564/

increased intracellular calcium has been modeled by [2,17–19]. The electrophysiology of the slow wave activity in the ICC was modeled in [20]. Models that describe the reactions that lead from increased calcium to MLC phosphorylation have been developed in [14,21]. In [14], the authors couple this MLC phosphorylation model to a model of actin-myosin force generation developed by Hai and Murphy [22]. In terms of cell models of muscle cell contraction, the most common types are those which simulate the whole cell as a continuum (individual fibers and cellular components not modeled) [23–25] or focus on modeling one actin-myosin stress fiber unit or sarcomere [26,27]. These models are generally based on Hill's three-element model [28] with the contractile element modeled using Huxley's sliding filament theory [29,30]. Examples of cell models developed to model other types of cell motion that simulate individual fibers and/or individual cellular components include [31,32] for modeling cell motility and [33–35] for modeling cellular deformations. The cell model developed in this work includes the simulation of individual actin-myosin stress fibers, cytoskeletal fibers, and the cell membrane. This type of model was adapted from previous work in [33].

In this paper we present a framework for a comprehensive model of ISMC contraction. As described above many models have been developed to simulate each subprocess. The models utilized in the demonstration of this framework were chosen so as to be useful for modeling the effects of intestinal edema. However one can easily replace any of the subprocess models with other models to accommodate other situations. This framework includes coupled models of: (1) the biochemical reaction system that leads to an increase in intracellular Ca^{2+} in the ISMC, (2) the reactions which link Ca^{2+} to MLC phosphorylation, (3) the conversion of phosphorylated MLC into mechanical force, and (4) a cell model of the mechanical contraction–relaxation of the ISMC including the simulation of cytoskeletal fibers, actin-myosin contractile fibers, the cell membrane, and the damping effects of cellular fluid.

The rest of the paper is organized as follows. We first present the details of the mathematical models for each portion of the contraction process, along with relevant biological background, parameter values, and descriptions of how the subprocess models communicate. We then present numerical results from the model for normal intestinal conditions and edematous conditions. The results are then discussed and compared to the experimental findings of Uray et al. [8]. The paper concludes with a summary of the framework and description of future work, which will include the extension of the model to several coupled ISMCs.

2. Mathematical model

This comprehensive model of ISMC contraction is comprised of several linked, subprocess models. We present here a description of these models and explain how information passes between them.

There are four subprocess models linked together in this overall model of ISMC contraction. Fig. 2 shows a flow chart of the four processes and the input data that flows from one process to the next. It should be noted that these four models are being simulated concurrently, with each model receiving new input data from the other models at each time step.

2.1. Calcium dynamics

The generation of force in an ISMC is dependent upon the level of intracellular free Ca^{2+} in the cell [14]. The level of Ca^{2+} increases when the ISMC membrane is depolarized by the passage of the slow wave in local ICC [14]. Even, it is still inconclusive whether a voltage-dependent IP_3 mechanism truly mediates Ca^{2+} transient in gastrointestinal tissues, a number of studies have demonstrated that an inositol 1,4,5-trisphosphate (IP_3), a signal transduction messenger molecule, mediated intracellular calcium level (Ca^{2+}) [36,37]. Different concentrations of an external stimulus (acetylcholine, ACh) are known to increase IP_3. Activated IP_3 stimulates the release of Ca^{2+} from the sarcoplasmic reticulum (SR), and these calcium ions work as a positive feedback mechanism in the release of more Ca^{2+} from the inner sarcoplasmic space, in a process known as calcium-induced calcium release (CICR) [19]. The increased calcium concentration affects the membrane potential of the cell along with potassium (K^+) channels embedded in the plasma membrane [38]. Both the membrane potential and K^+ channels regulate Ca^{2+} as well.

We utilize a combination of models to simulate calcium dynamics. The ordinary differential equation (ODE) that describes the changes in IP_3 over time [19] is given by:

$$\frac{d[IP_3]}{dt} = \beta - \epsilon[IP_3] - \frac{V_{M4}[IP_3]^u}{[IP_3]^u + K_4^u} + P_{MV}\left(1 - \frac{[E]^{r_2}}{K_V^{r_2} + [E]^{r_2}}\right) \tag{1}$$

IP_3 can be modulated by external stimuli (such as application of ACh), denoted by the term β. The concentration β is utilized as input data for the μM/min term β in Equation (1). The rest of the equations given below were adapted from [38] which is to the best of our knowledge the most advance model of SMCs and with Equation (1) form a set of five ODEs for five unknowns: IP_3, Ca_{SR} (calcium concentration in the SR), W (the open state probability of calcium-activated potassium channels), E (the cell membrane potential) and Ca_2 (free Ca^{2+} ions):

$$\frac{d[Ca_{SR}]}{dt} = \frac{B[Ca_2]^2}{[Ca_2]^2 + C_b^2} - \frac{C[Ca_{SR}]^2[Ca_2]^4}{([Ca_{SR}]^2 + s_c^2)([Ca_2]^4 + c_c^4)} - L[Ca_{SR}] \tag{2}$$

$$\frac{d[W]}{dt} = \lambda\left(\frac{([Ca_2] + c_W)^2}{([Ca_2] + c_W)^2 + \delta e^{-\left(\frac{[E]-v_{Ca_3}}{R_K}\right)}} - [W]\right) \tag{3}$$

$$\frac{d[E]}{dt} = \gamma\left(-F_{NaK} - G_{Cl}([E] - v_{Cl}) - \frac{2G_{Ca}([E] - v_{Ca_1})}{1 + e^{-\left(\frac{[E]-v_{Ca_2}}{R_{Ca}}\right)}} - G_{NCX}\frac{[Ca_2]([E] - v_{NCX})}{[Ca_2] + c_{NCX}} - G_K[W]([E] - v_K)\right) \tag{4}$$

$$\frac{d[Ca_2]}{dt} = \frac{F[IP_3]^2}{[IP_3]^2 + K_r^2} - \frac{G_{Ca}([E] - v_{Ca_1}}{1 + e^{-\left(\frac{[E]-v_{Ca_2}}{R_{Ca}}\right)}} + \frac{G_{NCX}[Ca_2]([E] - v_{NCX})}{[Ca_2] + c_{NCX}} - \frac{B[Ca_2]^2}{[Ca_2]^2 + C_b^2} + \frac{C[Ca_{SR}]^2[Ca_2]^4}{([Ca_{SR}]^2 + s_c^2)([Ca_2]^4 + c_c^4)} - D[Ca_2]\left(1 + \frac{([E] - v_d)}{R_d}\right) + L[Ca_{SR}] \tag{5}$$

All parameter descriptions and values for Equations (1)–(5) are given in Table 1. This set of ODEs is integrated in time utilizing a fourth-order Runge–Kutta method.

2.2. MLC phosphorylation

The increase in Ca^{2+} leads to the activation of myosin light chain kinase (MLCK) which in turn leads to MLC phosphorylation. MLC phosphorylation is necessary for smooth muscle contraction and the amount of force generated in smooth muscle is related to the degree of MLC phosphorylation [39,40]. We utilize the nine reactions given in Table 1 of [14] for this portion of the model. These reactions can be translated into a system of ODEs of the form $y_t = f(y, t)$ that tracks the levels of the nine chemicals stored in vector y over time. Quantities that are tracked include calcium, the enzyme calmodulin, MLCK and

Table 1
List of parameter values for the calcium dynamics model.

	Value	Description	Reference
$[IP_3]_0$	0.397 μM	Initial IP_3 concentration	[19]
$[Ca^{2+}_{SR}]_0$	1.1 μM	Initial SR calcium concentration	[38]
$[W]_0$	0.1	Initial potassium channel probability concentration	[38]
$[E]_0$	−42 mV	Initial cell potential	[38]
$[Ca^{2+}]_0$	0.19 μM	Initial intracellular calcium concentration	[38]
δ	0.13 μM^2	Translation factor	[48]
$\gamma =$	1970 mV/μM	Scaling factor	[48]
ϵ	0.015 s^{-1}	Rate constant for linear IP_3 degradation	[19]
λ	45	Channel constant	[48]
B	2.025 μM/s	SR uptake rate constant	[38]
C	55 μM/s	CICR rate constant	[38]
D	0.24 s^{-1}	Ca^{2+} Extrusion by ATPase rate constant	[38]
F	0.23 μM/s	Max influx rate of Ca^{2+}	[38]
L	0.025 s^{-1}	Leak from SR rate constant	[38]
C_b	1 μM	Half point of SR ATPase activation sigmoidal	[48]
c_c	0.9 μM	Half point of CICR activation sigmoidal	[38]
c_{NCX}	0.5 μM	Half point Na^+/Ca^{2+} exchange activation by Ca^{2+}	[38]
c_W	0.0 μM	Translation factor for Ca^{2+}	[48]
F_{NaK}	0.0432 μM/s	Net whole cell flux via the $Na^+ - K^+ -$ ATPase	[38]
G_{Ca}	0.00129 $\mu M mV^{-1} s^{-1}$	Whole cell conductance for VOCCs	[38]
G_{Cl}	0.00134 $\mu M mV^{-1} s^{-1}$	Whole cell conductance Cl	[38]
G_K	0.00446 $\mu M mV^{-1} s^{-1}$	Whole cell conductance K	[38]
G_{NCX}	0.00316 $\mu M mV^{-1} s^{-1}$	Whole cell conductance for Na^+/Ca^{2+} exchange	[38]
K_4	0.5 μM	Half saturation constant IP_3 degradation	[38]
K_r	1 μM	Half saturation constant Ca entry	[38]
K_V	−58 mV	Half saturation constant IP_3 voltage synthesis	[38]
P_{MV}	0.01333 $\mu M s^{-1}$	Max rate voltage IP_3 synthesis	[38]
R_2	8	Hill coefficient	[19]
R_{Ca}	8.5 mV	Maximum slope of VOCC activation	[38]
R_d	250.0 mV	S voltage dependence	[38]
R_K	12.0 mV	Maximum slope Ca activation	[38]
s_c	2 μM	Half point CICR efflux	[38]
u	4	Hill coefficient	[19]
v_{Ca_1}	100.0 mV	Reversal potential VOCCs	[38]
v_{Ca_2}	−24 mV	Half point VOCC activation	[38]
v_{Ca_3}	−27 mV	Half point Ca^{2+} channel activation	[38]
v_{Cl}	−25 mV	Reversal potential Cl	[38]
v_d	−100.0 mV	Intercept voltage dependence	[38]
v_K	−104.0 mV	Reversal potential K	[38]
V_{M4}	0.0333 $\mu M s^{-1}$	Max nonlinear IP_3 degradation	[19]
v_{NCX}	−40.0 mV	Reversal potential Na^+/Ca^{2+} exchange	[38]

various complexes of these three chemicals. A complex of four calcium ions, one calmodulin, and one MLCK (denoted $Ca_4C\,M_k$) is the activated complex that phosphorylates the regulatory myosin light-chain located at the base of the myosin head. Once activated, this head can bind with ATP to initiate the cross-bridge cycling necessary for contraction [14,41]. The full set of ODEs is:

$$\frac{d[C]}{dt} = r_1[Ca_2C] + r_3[CM_K] + r_8[CB_P] - f_1[Ca_2][C] - f_3[C][M_K] - f_8[C][B_P] \quad (6)$$

$$\frac{d[M_K]}{dt} = r_3[CM_K] + r_4[Ca_2CM_K] + r_5[Ca_4CM_K] - f_3[C][M_K] - f_4[M_K][Ca_2C] - f_5[M_K][Ca_4C] \quad (7)$$

$$\frac{d[Ca_2C]}{dt} = f_1[Ca_2][C] + r_2[Ca_4C] + r_4[Ca_2CM_K] + f_9[Ca_2][CB_P] - r_1[Ca_2C] - f_2[Ca_2][Ca_2C] - f_4[M_K][Ca_2C] - r_9[Ca_2C][B_P] \quad (8)$$

$$\frac{d[Ca_4C]}{dt} = f_2[Ca_2][Ca_2C] + r_5[Ca_4CM_K] - r_2[Ca_4C] - f_5[M_K][Ca_4C] \quad (9)$$

$$\frac{d[CM_K]}{dt} = f_3[C][M_K] + r_6[Ca_2CM_K] - r_3[CM_K] - f_6[Ca_2][CM_K] \quad (10)$$

$$\frac{d[Ca_2CM_K]}{dt} = f_4[M_K][Ca_2C] + f_6[Ca_2][CM_K] + r_7[Ca_4CM_K] - r_4[Ca_2CM_K] - r_6[Ca_2CM_K] - f_7[Ca_2][Ca_2CM_K] \quad (11)$$

$$\frac{d[Ca_4CM_K]}{dt} = f_5[M_K][Ca_4C] + f_7[Ca_2][Ca_2CM_K] - r_5[Ca_4CM_K] - r_7[Ca_4CM_K] \quad (12)$$

$$\frac{d[B_P]}{dt} = r_8[CB_P] + f_9[Ca_2][CB_P] - f_8[C][B_P] - r_9[Ca_2C][B_P] \quad (13)$$

$$\frac{d[CB_P]}{dt} = f_8[C][B_P] + r_9[Ca_2C][B_P] - r_8[CB_P] - f_9[Ca_2][CB_P] \quad (14)$$

A description of each component in these equations can be found in [14], as well as the values for all forward (f_i) and reverse (r_i) reaction rates and all initial concentration levels for the nine components. The quantity $[Ca_2]$ (described by a function in [14]) is replaced in this equation set by the $Ca_2(t)$ solution of Equation (5) from the calcium dynamics model. As with the set of calcium dynamics ODEs, this system will be advanced forward in time with a fourth-order Runge–Kutta method.

2.3. Force generation

In this next stage, chemical reactions create mechanical forces. Phosphorylated myosin (M_p) binds to an actin thin filament (A),

forming the actomyosin complex AM_p. The complex AM_p catalyzes the breakdown of ATP into ADP and P_i (inorganic phosphate), which leads to a conformational change in the myosin head. Once P_i is released from AM_p, the myosin head pulls the actin filament through the cytosol in an action termed the power-stroke. This motion is the moment of mechanochemical force generation, and the process continues cyclically during contraction [15]. This force production process can be captured in four ODEs, developed by Hai and Murphy [22] and adapted from [14]. The set is:

$$\frac{d[M]}{dt} = -\frac{k_1[Ca_4CM_K][M]}{k_2+[M]} + \frac{k_5[M_L][M_p]}{k_6+[M_p]} + k_7[AM] \tag{15}$$

$$\frac{d[M_p]}{dt} = \frac{k_1[Ca_4CM_K][M]}{k_2+[M]} - \frac{k_5[M_L][M_p]}{k_6+[M_p]} - k_3[M_p] + k_4[AM_p] \tag{16}$$

$$\frac{d[AM_p]}{dt} = k_3[M_p] - k_4[AM_p] + \frac{k_1[Ca_4CM_K][AM]}{k_2+[AM]} - \frac{k_5[M_L][AM_p]}{k_6+[AM_p]} \tag{17}$$

$$\frac{d[AM]}{dt} = -\frac{k_1[Ca_4CM_K][AM]}{k_2+[AM]} + \frac{k_5[M_L][AM_p]}{k_6+[AM_p]} - k_7[AM] \tag{18}$$

A description of each component and its value in these equations can be found in [14].

The amount of force generated by the actin-myosin stress fibers (denoted F_S) in the ISMC can be computed as [14]:

$$F_S = F_0\frac{[AM]+[AM_p]}{[M_p]+[AM_p]} \tag{19}$$

where F_0 is a scaling parameter. This force (which changes with time as the quantities AM, AM_p, and M_p evolve) will be utilized in the mechanical model described next.

2.4. Cell model of the ISMC

The final model included in this framework is a cell model of the ISMC that includes the cell membrane, cytoskeletal fibers, actin-myosin stress fibers, and the effects of cellular fluid drag. This cell model is a useful tool for exploring the effects of changes from the three chemical subprocess models on the ISMC's mechanical contraction.

The ISMC has a long spindle-shape, thus we will utilize its radial symmetry to obtain a two-dimensional model. The ISMC membrane is modeled by a one-dimensional, enclosed elastic string obeying a Hookean, stress (σ)–strain (ε) relationship: $\sigma = E_m\varepsilon$, where E_m is the membrane's Young's modulus, and the strain is defined as: $\varepsilon = \Delta L_M(t)/L_0$ with L_0 being the equilibrium length and $\Delta L_M(t)$ the change in length of the membrane at time t. The tension forces produced by the membrane over time are denoted by $F_M(t) = (E_m A_m \Delta L_M(t))/L_0$ where A_m is the area over which the stress is imposed. Attached to the membrane inside the periphery of the cell, is the cytoskeleton, represented here as one-dimensional actin filaments modeled as springs as done in previous work [33]. These cytoskeletal fibers provide tension forces $F_C(t) = (E_C A_C \Delta L_C(t))/L_0$ to the system, where similar to above, E_C is the fiber's Young's modulus, A_C is a fiber's cross-sectional area, $\Delta L_C(t)$ is the change in length from equilibrium of these fibers, and L_0 is the equilibrium length. Values for L_0 for both the membrane and the fibers are established by computing their initial lengths at the start of the simulation. The model also includes actin-myosin contractile fibers, that contract the cell with a sliding filament mechanism [10,15]. These stress fibers impose active contractile forces $F_S(t)$ on the system determined by the current level of phosphorylated MLC provided by the biochemical model described above. The motion of the three types of mechanical structures: membrane, cytoskeletal fibers, and actin-myosin fibers, is simulated over time with a large system of ODEs based on Newton's second law: $\sum F = m_i\ddot{\mathbf{x}}_i$, where the sum of F represents the sum of all forces acting on a particular discrete node point i at current position $\mathbf{x}_i = (x_i, y_i)$ within the discretized system, m_i is the mass of the node, and $\ddot{\mathbf{x}}_i$ is its acceleration. The system of ODEs for the cell system has the form:

$$m_i\ddot{\mathbf{x}}_i = F_M^i(t) + F_C^i(t) + F_S(t) - \delta\dot{\mathbf{x}}_i \tag{20}$$

where the term $-\delta\dot{\mathbf{x}}_i$ represents drag forces from the intracellular and extracellular fluid, with δ as the drag coefficient. The i superscripts on membrane and cytoskeletal fiber forces are present to indicate that these are calculated based on the current position of node i in the system. A diagram of the cell model is given in Fig. 1. Table 2 contains a list of values for the various parameters from the literature needed for this subprocess model. However, one caveat must be given. A typical cell contains on the order of 10^5–10^6 cytoskeletal and actin-myosin fibers [42]. Modeling all of these fibers is currently computationally intractable, thus we model a subset of this amount and adjust parameters of Table 2 to compensate for the reduced number of components.

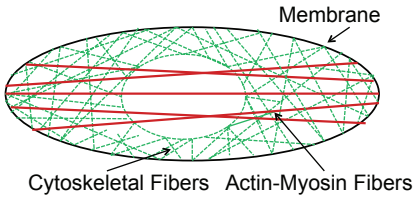

Fig. 1. Diagram (not to scale) of the components of the cell ISMC model.

Table 2
List of parameter values from the literature for the cell model. δ was computed using the cellular fluid viscosity, filament dimensions, and slender body theory.

	Value	Description	Reference
a	300 μm	ISMC's initial length	[41]
b	10 μm	ISMC's initial width	[41]
E_m	2.0×10^7 Pa	Membrane Young's modulus	Est. from [42]
E_C	2.0×10^9 Pa	Actin fiber Young's modulus	[42]
A_m	25 nm^2	2D cross-sectional area of membrane	Est. from [42]
A_C	100 nm^2	Actin filament cross-sectional area	[42]
δ	6.8×10^{-7} N · s/m	Cellular fluid drag coefficient	Est. from [49]
β_0	3.0135 μM	External stimulus generated IP_3	Current paper
β_1	1.8927 μM	External stimulus generated IP_3	Current paper
β_2	1.3476 μM	External stimulus generated IP_3	Current paper
β_3	1.0274 μM	External stimulus generated IP_3	Current paper
β_4	0.81874 μM	External stimulus generated IP_3	Current paper

3. Numerical experiments

To demonstrate the model's capabilities, we model a contraction–relaxation cycle of an ISMC under normal, non-edematous conditions, compared to several edematous condition simulations. The hypothesis being tested is that the excess fluid from edema that builds up in the interstitial spaces of the intestinal tissue creates larger distances, thereby reducing signal strength and consequently ISMC contractility.

We first set up the normal, non-edematous (NE) simulation by choosing $\beta = \beta_0$. For the edematous cases, all parameters remained the same as in the NE case, except for the values of β. We chose the values of β's as given in Table 2 so that the results produced in the subsequent chemical models would be similar to the results of [14], a model designed to simulate activity in a normal gastrointestinal smooth muscle cell. In the subsequent figures, these four edematous cases are labeled as β_1, β_2, β_3 and β_4.

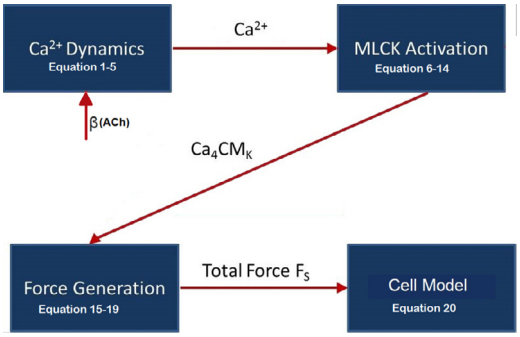

Fig. 2. Diagram of data flow between the four subprocess models.

4. Results

Fig. 3 shows the ISMC's Ca^{2+} concentration and the force generated by the phosphorylated MLC for the non-edematous and four edematous cases. The shapes and orders of magnitude of the non-edematous case curves (shown with solid black lines) are similar to those shown in [14] for both Ca^{2+} and force. The edematous cases have lower peak Ca^{2+} concentrations and peak force generation. It was expected that the Ca^{2+} and force data from the four cases would follow similar trends to the β data, however that is not the case. We observe a significant difference between the cases $\{\beta_0, \beta_1, \beta_2\}$ and the cases $\{\beta_3, \beta_4\}$ in both the Ca^{2+} and force data. There appears to be a threshold value for β below which there is a significant drop in Ca^{2+} concentration (and subsequently force generation). More analysis on this threshold phenomenon will be conducted in future work, however there is recent experimental evidence backing a threshold hypothesis (Karen Uray, Personal communication).

The peak Ca^{2+} concentrations in the ISMC for the four cases were: $Ca^{2+}_{\beta_0} = 1.1976\ \mu$M, $Ca^{2+}_{\beta_1} = 1.0978\ \mu$M, $Ca^{2+}_{\beta_2} = 0.9704\ \mu$M, $Ca^{2+}_{\beta_3} = 0.2453\ \mu$M, and $Ca^{2+}_{\beta_4} = 0.2247\ \mu$M. The force generated in the four cases were: $Fs_{\beta_0} = 8.0873$ mN, $Fs_{\beta_1} = 7.3696$ mN, $Fs_{\beta_2} = 6.4001$ mN, $Fs_{\beta_3} = 0.1836$ mN, and $Fs_{\beta_4} = 0.1338$ mN.

Fig. 4 conduct a phase analysis of Ca^{2+} concentration and the force generated at the non-edematous and four edematous cases. From that figure we can clearly see that there is a significant drop-off after β_2 in Ca^{2+} concentration and the force.

Finally, Fig. 5 contains snapshots in time of the physical cell undergoing contraction driven by the force values of Fig. 3. The left set of snapshots is from the NE case, while the right set is from the β_2 case. The five snapshots show the simulations at the beginning, halfway through contraction, full contraction, halfway through relaxation, and full relaxation. The times do not coincide since the β_2's contraction takes longer to get underway than the NE case. Fig. 6 shows a plot of the ISMC's major axis length versus time for the five cases, and also a bar graph of the maximum percent contraction of the ISMC in each case. This data reflect the same pattern as the force data. Cases β_0, β_1 and β_2 shown incremental drops in contractile activity,but then there is a significant drop-off in contraction in the β_3 and β_4 cases. The percentage in the reduction of the contraction for each case (Pc is computed as the difference between the original length and maximum contracted length divided by original length times 100) is: $Pc_{\beta_0} = 18.5\%$, $Pc_{\beta_1} = 13.4\%$, $Pc_{\beta_2} = 11.8\%$, $Pc_{\beta_3} = 0.4\%$, and $Pc_{\beta_4} = 0.3\%$.

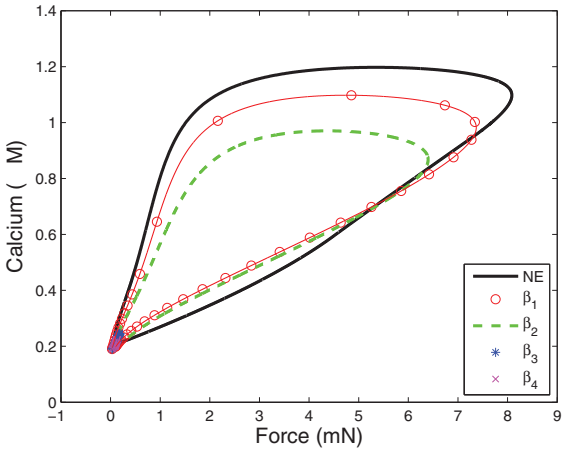

Fig. 4. A phase analysis of calcium concentration versus force generated for the five cases of β values.

To determine whether these results are reasonable, we utilize the data of [8]. In this study, small segments of intestinal smooth muscle tissue (both normal and edematous) taken from rats had their contractile activity measured. The edema case produced approximately 71.8% of the contractile activity that the normal tissue did (see Fig. 3 in [8]). The β_2 and β_3 cases produced approximately 72.4% and 63.8% of the contractile activity that the normal tissue did, so our results are quite reasonably in line with the experimental data.

5. Discussion

A comprehensive framework for modeling the biochemistry and mechanics of the ISMC contraction cycle has been developed. This framework consists of the coupling of four subprocess models, including the simulation of cellular calcium dynamics, MLC phosphorylation, actin-myosin force generation, and a model of the cell

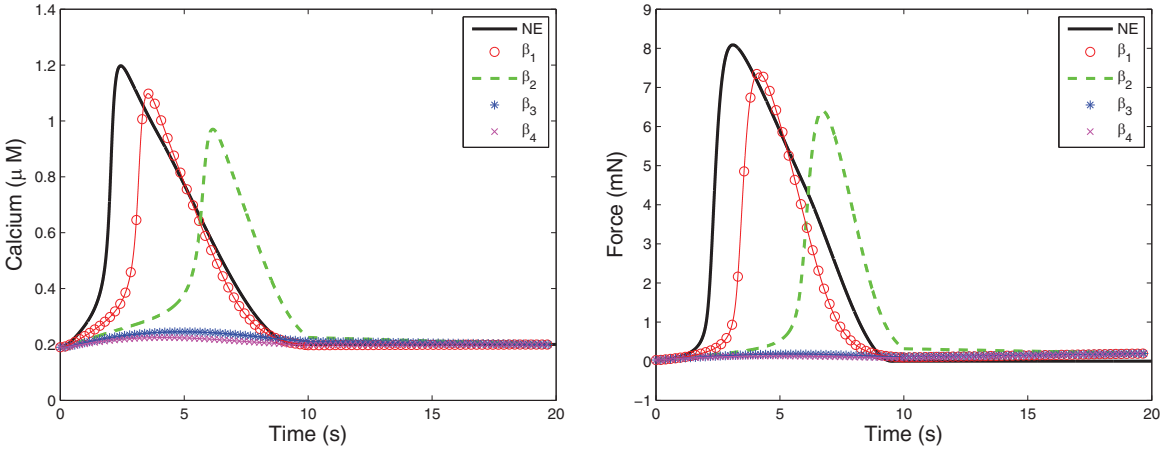

Fig. 3. Calcium concentration in the ISMC for the five cases versus time (left). Force generated by the ISMC for the five cases versus time (right).

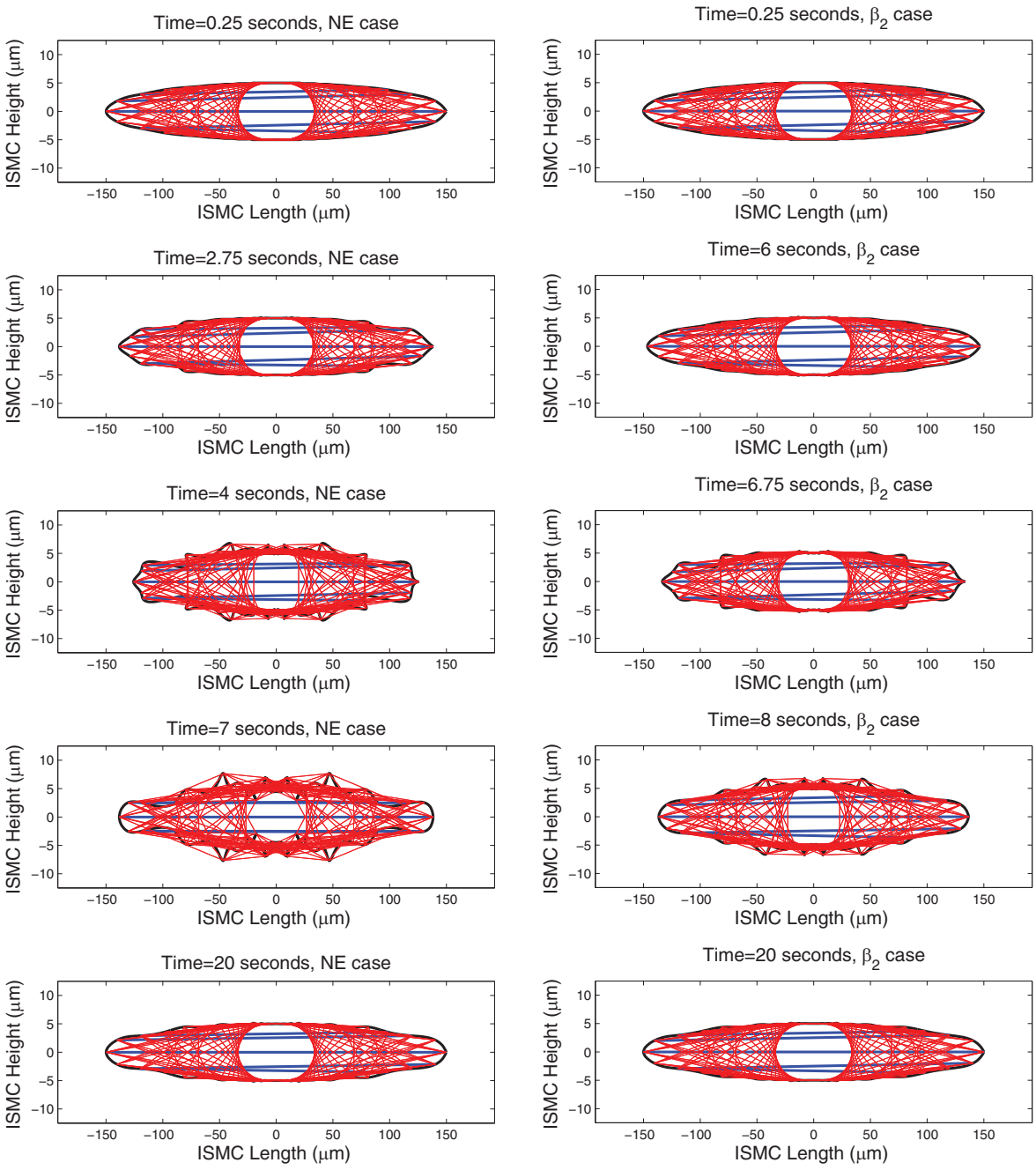

Fig. 5. Snapshots in time of the ISMC cell model at the simulation beginning, halfway through contraction, peak contraction, halfway through relaxation, and at the simulation's end, for the NE case (left column) and the edematous case for β_2 (right column).

contraction of the ISMC. This framework was developed in order to study the effects of intestinal edema on ISMC contractility. It has been shown experimentally that there is a correlation between increased edema and slowed contractility, however the cause is unknown. Our work tested the hypothesis that the amount of stimulus in the calcium dynamics has a direct effect on the muscle contractility. Simulation results showed that the ISMCs with an external stimulus had decreased contractile activity compared to the normal case. An interesting result was that the decrease in contractile activity did not vary in an incremental fashion with β, but rather beyond β_2 there was a significant drop-off. This phenomenon will be explored further in future work with our experimental collaborators.

The external stimuli, represented by β in our model, may correspond to acetylcholine (ACh) which is one of the neurotransmitters emitted from the neurons in the intestine. ACh diffuses across the synaptic cleft (approximately 15–30 nm in width under normal, non-edematous conditions [43,44]) and binds to receptors on the postsynaptic membrane. A smaller amount in β would mean that a smaller amount of ACh has reached the membrane receptors. A possible explanation for the decrease in the amount of ACh for the edematous cases is that there is a significant increase in interstitial fluid and this will result in an increase of the average synapse width to 30–60 nm [45].

In future work, the model will be extended to include several coupled ISMCs, and eventually to a continuum-level tissue model. These models will be linked to one another in a multi-scale fashion. In order to continue to improve the model and also provide further means of validation, our experimental collaborators plan to perform further experiments, including the measurement of synapse widths in normal versus edematous tissue as well as experiments geared

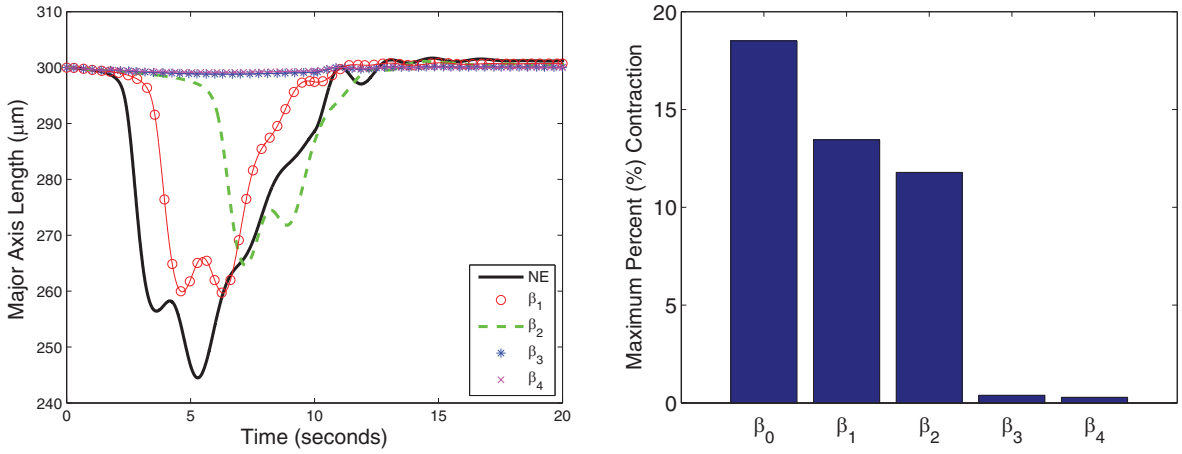

Fig. 6. The length of the major axis of the ISMC in μm versus time (left). The maximum percentage of reduction of contraction of the ISMC (right).

toward exploring a potential threshold of edema beyond which contractile activity is severely impaired. Also, the cell model will be explored replacing this purely discrete model with a multi-scale, continuum-discrete model (such as [46]) to allow for a higher level of detail at reasonable computational costs.

The goal for this initial research effort was to combine several subprocess models, which describe portions of ISMC contractility, into a linked framework in order to study the entire process. The original motivation for its development was for studying intestinal edema, however the model will be valuable for exploring the effects of other gastrointestinal diseases or impairments on intestinal motility. It is possible that the reduced intestinal motility associated with edema could be a multi-factorial problem. For example, it is also known that; viral infections of the intestines may lead to inflammation that particularly damages the ICC, and the ICC are now known to play an important role in gut motility and absent or disordered ICC networks have been identified in a variety of motility disorders [47].

Acknowledgement

The authors thank Isadora Calderon, Andrew Ferguson and Andria Remirez for their useful discussions.

References

[1] R. Miftahof, H.G. Nam, D.L. Wingate, Mathematical Modeling and Simulation in Enteric Neurobiology, World Scientific Pub Co. Inc., 2009.
[2] A. Corrias, M.L. Buist, A quantitative model of gastric smooth muscle cellular activation, Annal. Biomed. Eng. 35 (9) (2007) 1595–1607.
[3] R.M. Dongaonkar, C.M. Quick, R.H. Stewart, R.E. Drake, C.S. Cox Jr., G.A. Laine, Edemagenic gain and interstitial fluid volume regulation, Am. J. Physiol.-Reg. I 294 (2) (2008) R651–R659.
[4] D.N. Granger, J. Barrowman, Gastrointestinal and liver edema, in: N.C. Staub, A.E. Taylor (Eds.), Edema, Raven Press, 1984, pp. 615–656.
[5] S.D. Moore-Olufemi, J. Padalecki, S.E. Olufemi, H. Xue, D.H. Oliver, R.S. Radhakrishnan, S.J. Allen, F.A. Moore, R. Stewart, G.A. Laine, et al., Intestinal edema: Effect of enteral feeding on motility and gene expression, J. Surg. Res. 155 (2) (2009) 283–292.
[6] C.S. Cox Jr., R. Radhakrishnan, L. Villarrubia, H. Xue, K. Uray, B.S. Gill, R.H. Stewart, G.A. Laine, Hypertonic saline modulation of intestinal tissue stress and fluid balance, Shock 29 (5) (2008) 598–602.
[7] S. Moore-Olufemi, H. Xue, S. Allen, F. Moore, R. Stewart, G. Laine, C. Cox, Inhibition of intestinal transit by resuscitation-induced gut edema is reversed by $l-nil^{1,2}$, J. Surg. Res. 129 (1) (2005) 1–5.
[8] K.S. Uray, G.A. Laine, H. Xue, S.J. Allen, C.S. Cox Jr., Intestinal edema decreases intestinal contractile activity via decreased myosin light chain phosphorylation, Crit. Care Med. 34 (10) (2006) 2630–2637.
[9] K.S. Uray, G.A. Laine, H. Xue, S.J. Allen, C.S. Cox Jr., Edema-induced intestinal dysfunction is mediated by stat3 activation, Shock 28 (2) (2007) 239–244.
[10] H. Gregersen, Biomechanics of the Gastrointestinal Tract: New Perspectives in Motility Research and Diagnostics, Springer Verlag, 2003.
[11] C.D. Benham, T.B. Bolton, R.J. Lang, Acetylcholine activates an inward current in single mammalian smooth muscle cells, Nature 316 (1985) 345–347.
[12] M.J. Berridge, Smooth muscle cell calcium activation mechanisms, J. Physiol. 586.21 (2008) 5047–5061.
[13] M.B. Vivaudou, L.H. Clapp, J.V. Walsh, J.J. Singer, Regulation of one type of ca^2 current in smooth muscle cells by diacyiglycerol and acetylcholine, FASEB J. 2 (9) (1988) 2497–2504.
[14] V. Gajendiran, M.L. Buist, A quantitative description of active force generation in gastrointestinal smooth muscle, Int. J. Numer. Method Biomed. Eng. 27 (3) (2011) 450–460.
[15] B. Alberts, D. Bray, J. Lewis, M. Raff, K. Roberts, J.D. Watson, Molecular Biology of the Cell, second ed., Garland Science, 1994.
[16] T.D. Pollard, W.C. Earnshaw, Cell Biology, second ed., Elsevier, 2008.
[17] R. Miftakhov, G. Abdusheva, Numerical simulation of excitation-contraction coupling in a locus of the small bowel, Biol. Cyber. 74 (5) (1996) 455–467.
[18] P. Du, Y. Poh, J. Lim, V. Gajendiran, G. O'Grady, M. Buist, A. Pullan, L. Cheng, A preliminary model of gastrointestinal electromechanical coupling, IEEE Trans. Biomed. Eng. 58 (12) (2011) 3491–3495.
[19] M.S. Imtiaz, D.W. Smith, D.F. Van Helden, A theoretical model of slow wave regulation using voltage-dependent synthesis of inositol 1, 4, 5-trisphosphate, Biophys. J. 83 (4) (2002) 1877–1890.
[20] A. Corrias, M.L. Buist, Quantitative cellular description of gastric slow wave activity, Ann. J. Physiol. Gastrointest. Liver Physiol. 294 (2008) G985–G995.
[21] T.J. Lukas, A signal transduction pathway model prototype II: Application to ca2+-calmodulin signaling and myosin light chain phosphorylation, Biophys. J. 87 (3) (2004) 1417–1425.
[22] C.M. Hai, R.A. Murphy, Cross-bridge phosphorylation and regulation of latch state in smooth muscle, Am. J. Physiol.–Cell Physiol. 254 (1) (1988) C99–C106.
[23] A.S. Wexler, J. Ding, S.A. Binder-Macleod, A mathematical model that predicts skeletal muscle force, IEEE Trans. Biomed. Eng. 44 (5) (1997) 337–348.
[24] A.Y.K. Wong, Mechanics of cardiac muscle, based on huxley's model: mathematical simulation of isometric contraction, J. Biomech. 4 (6) (1971) 529–540.
[25] W. Williams, Huxleys model of muscle contraction with compliance, J. Elasticity 105 (1) (2011) 365–380.
[26] F.M. Montevecchi, R. Pietrabissa, A model of multicomponent cardiac fibre, J. Biomech. 20 (4) (1987) 365–370.
[27] E. Pate, R. Cooke, A model of crossbridge action: The effects of atp, adp and p i, J. Muscle Res. Cell Motility 10 (3) (1989) 181–196.
[28] A. Hill, The heat of shortening and the dynamic constants of muscle, Proc. Roy. Soc. London B, Biol. Sci. 126 (843) (1938) 136–195.
[29] A. Huxley, Muscular contraction, J. Physiol. 243 (1) (1974) 1–43.
[30] A.F. Huxley, et al., Muscle structure and theories of contraction, Prog. Biophys. Biophys. Chem. 7 (1957) 255–318.
[31] B. Rubinstein, K. Jacobson, A. Mogilner, Multiscale two-dimensional modeling of a motile simple-shaped cell, Multi. Model. Simul. 3 (2005) 413–439.
[32] D.C. Bottino, L.J. Fauci, A computational model of ameboid deformation and locomotion, Eur. Biophys. J. 27 (5) (1998) 532–539.
[33] J. Young, S. Mitran, A numerical model of cellular blebbing: A volume-conserving, fluid-structure interaction model of the entire cell, J. Biomech. 43 (2) (2010) 210–220.
[34] D.E. Discher, D.H. Boal, S.K. Boey, Simulations of the erythrocyte cytoskeleton at large deformation. II. Micropipette aspiration, Biophys. J. 75 (3) (1998) 1584–1597.
[35] J. Li, M. Dao, C.T. Lim, S. Suresh, Spectrin-level modeling of the cytoskeleton and optical tweezers stretching of the eruthrocyte, Biophys. J. 88 (2005) 3707–3719.
[36] K.M. Sanders, S.D. Koh, S.M. Ward, Interstitial cells of cajal as pacemakers in the gastrointestinal tract, Annu Rev. Physiol. 68 (2006) 307–343.
[37] P. Du, G. O'Grady, S.J. Gibbons, R. Yassi, R. Lees-Green, G. Farrugia, L.K. Cheng, A.J. Pullan, Tissue-specific mathematical models of slow wave entrainment in wild-type and $5-ht_{2B}$ knockout mice with altered interstitial cells of cajal networks, Biophys. J. 98 (9) (2010) 1772–1781.
[38] M. Koenigsberger, R. Sauser, M. Lamboley, J.L. Bény, J.J. Meister, Ca2+ dynamics in a population of smooth muscle cells: Modeling the recruitment and synchronization, Biophys. J. 87 (1) (2004) 92–104.

[39] K.E. Kamm, J.T. Stull, The function of myosin and myosin light chain kinase phosphorylation in smooth muscle, Annu. Rev. Pharmacol. Toxicol. 25 (1) (1985) 593–620.
[40] A.P. Somlyo, A.V. Somlyo, Signal transduction and regulation in smooth muscle, Nature 372 (6503) (1994) 231–236.
[41] F. Schroeder, W. Wood, A. Kier, in N. Sperelakis (Ed.), Cell Physiology Sourcebook: A Molecular Approach, Academic Press, New York, 2001.
[42] D. Boal, Mechanics of the Cell, Cambridge University Press, 2002.
[43] L.P. Savtchenko, D.A. Rusakov, The optimal height of the synaptic cleft, Proc. Natl. Acad. Sci. 104 (6) (2007) 1823–1828.
[44] C.E. Devine, F.O. Simpson, W.S. Bertraud, Freeze-etch studies on the innervation of mesenteric arteries and vas deferens, J. Cell. Sci. 9 (1971) 411–425.
[45] J. Young, B. Rivière, C.S. Cox Jr., K. Uray, A mathematical model of intestinal oedema formation, Math. Med. Biol. 31 (1) (2014) 1–15.
[46] J. Young, S. Mitran, A continuum-microscopic algorithm for modeling fibrous, heterogeneous media with dynamic microstructures, Multi. Model. Simul. 9 (2011) 241–257.
[47] C.J. Streutker, J.D. Huizinga, D.K. Driman, R.H. Riddell, Interstitial cells of cajal in health and disease. Part I: Normal ICC structure and function with associated motility disorders, Histopathology 50 (2007) 176–189.
[48] D. Parthimos, D. Edwards, T. Griffith, Minimal model of arterial chaos generated by coupled intracellular and membrane ca2+ oscillators, Am. J. Physiol.—Heart Circulat. Physiol. 277 (3) (1999) H1119–H1144.
[49] G.T. Charras, M. Coughlin, T.J. Mitchison, L. Mahadevan, Life and times of a cellular bleb, Biophys. J. 94 (5) (2008) 1836–1853.